Geophysical Research Letters

RESEARCH LETTER
10.1029/2020GL091899

Key Points:

- Warming of the subtropical gyre at depth strengthens the subsurface heat transport from the subtropical gyre to the subpolar gyre
- Precession-paced northward heat transport may affect ice-sheet mass balance by either contributing moisture or triggering destabilization
- Onset of precession-paced northward heat transport began around 930 ka, promoting the transition to 100-kyr cyclicity

Supporting Information:

Supporting Information may be found in the online version of this article.

Correspondence to:

M. C. A. Catunda,
carolina.catunda@geow.uni-heidelberg.de

Citation:

Catunda, M. C. A., Bahr, A., Kaboth-Bahr, S., Zhang, X., Foukal, N. P., & Friedrich, O. (2021). Subsurface heat channel drove sea surface warming in the high-latitude North Atlantic during the Mid-Pleistocene Transition. *Geophysical Research Letters*, *48*, e2020GL091899. https://doi.org/10.1029/2020GL091899

Received 29 NOV 2020
Accepted 16 MAY 2021

Author Contributions:

Conceptualization: André Bahr, Oliver Friedrich
Data curation: M. Carolina A. Catunda
Formal analysis: M. Carolina A. Catunda, André Bahr, Xu Zhang, Nicholas P. Foukal
Funding acquisition: André Bahr

Subsurface Heat Channel Drove Sea Surface Warming in the High-Latitude North Atlantic During the Mid-Pleistocene Transition

M. Carolina A. Catunda[1], André Bahr[1], Stefanie Kaboth-Bahr[2,1], Xu Zhang[3,4], Nicholas P. Foukal[5], and Oliver Friedrich[1]

[1]Institute of Earth Sciences, Heidelberg University, Heidelberg, Germany, [2]Institute of Geosciences, University of Potsdam, Potsdam-Golm, Germany, [3]Key Laboratory of Western China's Environmental Systems (Ministry of Education), College of Earth and Environmental Science, Lanzhou University, Lanzhou, China, [4]CAS Center for Excellence in Tibetan Plateau Earth Sciences, Chinese Academy of Sciences, Beijing, China, [5]Department of Physical Oceanography, Woods Hole Oceanographic Institution, Woods Hole, MA, USA

Abstract The Mid-Pleistocene Transition (MPT, 1,200–600 ka) marks the rapid expansion of Northern Hemisphere (NH) continental ice sheets and stronger precession pacing of glacial/interglacial cyclicity. Here, we investigate the relationship between thermocline depth in the central North Atlantic, subsurface northward heat transport and the initiation of the 100-kyr cyclicity during the MPT. To reconstruct deep-thermocline temperatures, we generated a Mg/Ca-based temperature record of deep-dwelling (~800 m) planktonic foraminifera from mid-latitude North Atlantic at Site U1313. This record shows phases of pronounced heat accumulation at subsurface levels during the mid-MPT glacial driven by increased outflow of the Mediterranean Sea. Concurrent warming of the subtropical thermocline and subpolar surface waters indicates enhanced (subsurface) inter-gyre transport of warm water to the subpolar North Atlantic, which provided moisture for ice-sheet growth. Precession-modulated variability in the northward transport of subtropical waters imprinted this orbital cyclicity into NH ice-sheets after Marine Isotope Stage 24.

Plain Language Summary Large continental ice-sheets are a key component of the Earth's climate system, yet the factors controlling their build-up and destabilization on geological time-scales are far from understood. One of the remarkable aspects of Pleistocene (2.58 Ma to 11.65 ka) ice-sheets is that they appear to be highly sensitive to low-latitude forcing, a teleconnection that is yet not well-understood. In this study, we investigate if changes in the subsurface transport of heat from the subtropics into the high latitude North Atlantic may have played an overlooked role in controlling ice-sheet size. To address this issue, we obtained a new record of upper ocean temperature distribution in the North Atlantic during the Mid-Pleistocene Transition (MPT, 1200–600 ka), a period when ice-sheets expanded and our climate system shifted to longer glacial cycles. Our data reveal distinct pulses of low-latitude heat that were transported northwards by the ocean, warming the surface of the high-latitude North Atlantic during cold stages of prominent ice-sheet build-up. These anomalously warm surface waters may have provided excess moisture to the adjacent ice-sheets. Thus, we suggest that subsurface transport of warm and salty waters northward imprinted low-latitude variability into high-latitude ice sheets starting during the MPT.

1. Introduction

Between 1.2 and 0.6 Ma, the character of the glacial/interglacial cyclicity shifted from a 41-kyr period to the ~100-kyr long, saw-toothed cycles characteristic of the Late Pleistocene (Imbrie et al., 1993; Ruddiman et al., 1989). This cyclicity shift involved profound changes in the climatic system such as larger glacial ice-sheets (Berger & Jansen, 1994; Raymo, 1997), an abrupt drop in glacial atmospheric CO_2 (Hönisch et al., 2009), and more pronounced precession pacing of the glacial/interglacial rhythm (Imbrie et al., 1993). Although there have been numerous studies on the Mid-Pleistocene Transition (MPT) (e.g., Clark et al., 2006; McClymont et al., 2013), the mechanisms responsible for the cyclicity shift in the absence of significant change in the orbital configuration remain elusive.

Investigation: M. Carolina A. Catunda, André Bahr, Stefanie Kaboth-Bahr, Nicholas P. Foukal
Methodology: M. Carolina A. Catunda, André Bahr, Xu Zhang
Resources: André Bahr, Oliver Friedrich
Software: Xu Zhang
Supervision: André Bahr, Oliver Friedrich
Visualization: M. Carolina A. Catunda, André Bahr, Xu Zhang
Writing – original draft: M. Carolina A. Catunda, André Bahr, Stefanie Kaboth-Bahr, Nicholas P. Foukal, Oliver Friedrich
Writing – review & editing: M. Carolina A. Catunda, André Bahr, Stefanie Kaboth-Bahr, Xu Zhang, Oliver Friedrich

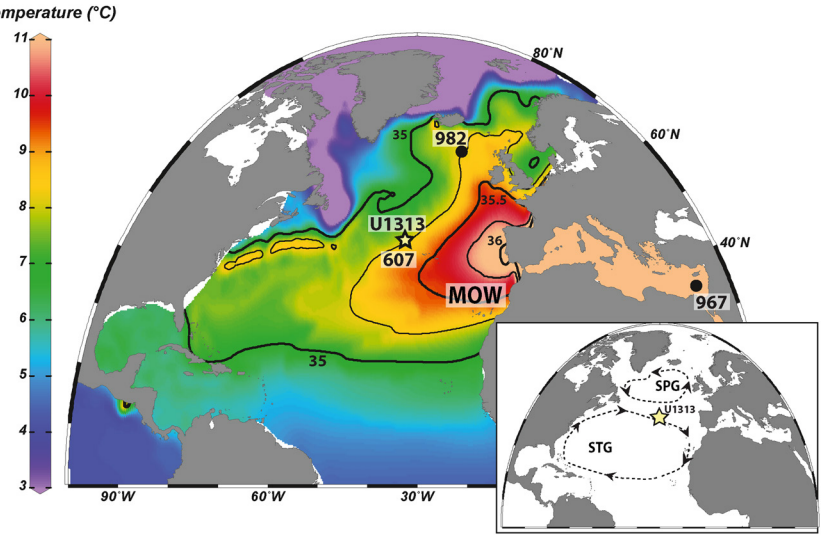

Figure 1. (main) Temperature along the $\sigma_0 = 27.45$ surface, which intersects Site U1313 (star) at 800 m depth (Locarnini et al., 2019). Black contours indicate isohalines from 35 to 36 psu at 0.25 intervals (Zweng et al., 2019). (inset) Location of Site U1313 (star) relative to the Subtropical Gyre (STG) and the Subpolar Gyre (SPG).

Early studies on the MPT have suggested that the increase in precession forcing, typical for low-latitude climate variability, on high-latitude ice-sheets may be explained by the southward migration of the continental edges of Northern Hemisphere (NH) ice-sheets (Ruddiman & McIntyre, 1981). However, reconstructions of the Laurentide ice-sheet (LIS) meltwater discharges suggested that the LIS frequently expanded into mid-latitudes already in the Early Pleistocene, and even though precession-modulated NH summer insolation strongly influenced these expansions, it had apparently little impact on the overall obliquity-paced glacial/interglacial cyclicity (Shakun et al., 2016). Ruddiman et al. (1989) proposed that high-latitude ice sheets may have become more sensitive to precessional insolation heating of low- and mid-latitude land masses south of the ice sheets, but why and how this change would have happened during the MPT remained unclear. Although there appears to be a strong influence of precession-forced oceanic heat and moisture transport to the European and British ice sheets during the last two glacials (Kaboth-Bahr et al., 2018), it remains uncertain whether this relates to ice-sheet variability across the MPT. Understanding the climatic mechanisms supporting low-latitude influence on ice-accumulation and ice-sheet instability in the NH is therefore important, as it can provide important clues about the origin of the MPT.

The dynamics of NH ice-sheets are intimately linked to variations in ocean circulation on millennial and orbital timescales (Hodell & Channell, 2016; Zhang et al., 2014). The upper ocean provides a direct source of heat and moisture to the atmosphere, thus impacting the mass balance of the adjacent ice-sheets. The strength of the heat transport into the North Atlantic depends on the transfer of accumulated warm waters from the mid-latitude Subtropical Gyre (STG) to the high-latitude Subpolar Gyre (SPG, Bower et al., 2019; Broecker, 1991). Recent modeling and drifter studies on North Atlantic inter-gyre exchange indicate that communication between the gyres at the surface is limited due to southward Ekman velocities and a strong surface potential vorticity gradient (Burkholder & Lozier, 2014). As these constraints on the inter-gyre connectivity decrease with depth, a more direct pathway exists for water stored within the subsurface STG to flow northwards along density surfaces (isopycnals) that outcrop in the high-latitude North Atlantic (Foukal & Lozier, 2016). The discovery of this subsurface route implies that subtropical water is transmitted to higher latitudes from deeper water depths than previously expected. Maximum flow was found along the $\sigma_0 = 27.1$ isopycnal, which currently lies between 400 and 500 m in the modern central North Atlantic (Burkholder & Lozier, 2011). Hence, northward heat transport via subsurface routes may have played a so far neglected role in oceanographic processes, including the boundary conditions leading to the MPT.

Here, we report on a new subsurface temperature (SubT) record from Integrated Ocean Drilling Project (IODP) Site U1313 (41°N, 33°W, 3,426 m water depth, Figure 1) across the interval Marine Isotope Stage (MIS) 36 to 14 (~1.2–0.54 Ma). We calculate the surface-subsurface temperature gradient between SubT and

the sea-surface temperature (SST) record from the same core (Naafs et al., 2012). As vertical temperature gradients determine thermocline stratification in the region, these data allowed to reconstruct the geometric configuration of isopycnals in the upper ocean along the primary heat pathway between the STG and the SPG. We further assessed the connection between thermocline stratification and northward heat transport across the MPT by calculating the surface-temperature gradient between Site U1313 and subpolar Site 982 (Lawrence et al., 2010) ($\Delta SST_{U1313\text{-}982}$) located at northeastern North Atlantic (NENA). Based on our findings, we propose that subsurface heat transport played a vital role in enhancing the northward oceanic heat transport during the MPT, which might have helped shaping glacial/interglacial variability during Mid- and Late Pleistocene.

2. Current Hydrography of Site U1313

Site U1313 is ideally situated to track heat transport variability to the higher latitudes as it is located at the intersection between STG and SPG (Figure 1). At the surface, U1313 is within the North Atlantic Current, characterized by saline and warm waters (~18°C). The uppermost 150 m of the water column at Site U1313 comprises the mixed layer (supporting text and Figure S1) and the seasonal thermocline (Locarnini et al., 2019; Zweng et al., 2019). The permanent thermocline, between 150 and 1,100 m, is extremely deep due to entrainment of Mediterranean Outflow Water (MOW) into central waters in the eastern North Atlantic (Spall, 1999) and contains the mode waters formed within the inter-gyre region and eastern SPG (Brambilla et al., 2008; García-Ibáñez et al., 2018). Eastern North Atlantic Central Waters of 12°C–16°C originate in the inter-gyre regions and occupy depths between 150 and 650 m. Between 650 and 1,100 m, the water column at Site U1313 is occupied by Subpolar Mode Waters (SPMW) formed in the Iceland and Irminger basins (Text S1). In the intermediate levels (1,100–2,000 m), fresh and oxygenated Labrador Sea Water mixes isopycnally with saline and warm MOW (Daniault et al., 1994) to form upper North Atlantic Deep Water (NADW). Below 2,000 m, the North Atlantic is dominated by the lower NADW.

To calculate SubT, we selected the foraminifera *Globorotalia crassaformis* that thrives at oxygen-depleted levels of the upper pycnocline (Kemle-von Mücke & Oberhänsli, 1999). At Site U1313, low-oxygen levels are found at ~800 m depth, at the deep thermocline, in agreement with the calculated calcification depth for this species in the subtropical North Atlantic (Cléroux et al., 2013). At this depth ($\sigma_0 = 27.45$), the water column is characterized primarily by SPMW (García-Ibáñez et al., 2018) and MOW that modulates temperature distribution at this density level in central North Atlantic (Figure 1 and Text S1).

3. Materials and Methods

3.1. Sampling and Sample Preparation

We used sediment samples of Site U1313, drilled in the central North Atlantic during IODP Expedition 306 (Figure 1). Sections from the primary splice were sampled every 5 cm between 26.82 adjusted composite depth in meters (amcd) and 56.77 amcd. The 10 cm^3 samples were freeze dried, weighted, wet sieved over >125 μm and >63 μm meshes, rinsed with Milli-Q water, and dried at 40°C. Around 15 tests (~750 μg) of the deep-dwelling foraminiferal species *G. crassaformis* were picked from a narrow size fraction (315–400 μm). Subsequently, the tests were cracked between glass plates, homogenized, and used for trace-element analyses. Tests of *Cibicidoides wuellerstorfi* and *Uvigerina peregrina* were picked, analyzed for stable isotopes, and used to update the Site U1313 age model (see supporting Text S2, Figure S3, and Table S1).

3.2. Mg/Ca Analyses

For Mg/Ca analyses, the cracked foraminiferal tests were cleaned following the procedures described by Martin and Lea (2002) without the diethylenetriaminepentaacetic acid (DTPA) step. This method includes a reduction step for the removal of metal-oxides with an ammonium citrate/hydrazine solution and an oxidation step with H_2O_2 for the removal of organic matter. A total of 540 trace-element analyses have been performed on a Thermo Scientific Agilent 720 ICP-OES at the Institute of Earth Sciences, Heidelberg University. Blanks were measured alongside the samples to exclude potential contamination during the cleaning

process. Standard deviation from replicates ($n = 20$) was ±0.14 mmol/mol for Mg/Ca, which would account for a temperature uncertainty of ±0.86°C using the species-specific Equation 1 (Cléroux et al., 2013).

$$\frac{\mathrm{Mg}}{\mathrm{Ca}} = 0.624 \pm 0.007\, e^{0.132 \pm 0.018 T} \quad (1)$$

Fe/Ca and Mn/Ca ratios were additionally analyzed to monitor contamination by siliciclastic material and diagenetic overgrowths. Mg/Ca, Fe/Ca, and Mn/Ca results were normalized to the external standard ECRM752-1 (3.762 mmol/mol for Mg/Ca, 0.17 mmol/mol for Fe/Ca, 0.132 mmol/mol for Mn/Ca, Greaves et al., 2008). Linear correlation between Fe/Ca and Mg/Ca was inferred as siliciclastic contamination and led to the exclusion of seven data points with Fe/Ca >0.2 mmol/mol. Linear correlation between Mn/Ca and Mg/Ca was interpreted as a sign of diagenetic overgrowth and led to the exclusion of further three data points with Mn/Ca >0.26 mmol/mol.

4. Results and Discussion

4.1. Subsurface Temperature and Thermocline Variability at Site U1313

The SubT record shows a glacial-interglacial pattern, which follows SST fluctuations at Site U1313 between MIS 36 and MIS 25 (Figures 2a and S4). From MIS 24 to 17, SubTs begin a long-term temperature increase interrupted by abrupt transitions to cold temperatures. Distinct SubT increases also preceded surface warming at the end of cold stages MIS 24, 22, and 20 (Figure S5), with a maximum lead of SubT relative to SST of ~22 kyr during MIS 22.

Our vertical temperature gradient Δ(SST-SubT) shows that a steep thermal gradient of 11.2 ± 1.9°C existed at Site U1313 for most of the time interval between 1.2 and 0.93 Ma (MIS 36–25; Figure 2b), which is higher than the modern mean annual gradient between surface and 800 m water depth of ~9.5°C (Locarnini et al., 2019) (for a discussion of the uncertainty of the Δ(SST-SubT) gradient, cf. Text S3). Between MIS 24 and MIS 17 (~0.93–0.67 Ma), SST cooling is opposed by warm SubTs, resulting in a prolonged phase of decreased stratification (9.1°C ± 1.5°C) that clearly separates this interval from short episodes of weak stratification occurring earlier in the record. This trend reversed only after MIS 17 (~0.67 Ma) when the steep thermal gradient was re-established.

Weak upper-ocean stratification between MIS 24 and 17 (Figure 2b) shows that the thermocline deepened in the mid-latitude North Atlantic and heat accumulated at subsurface levels. Minimum upper-ocean stratification occurred during MIS 24 (8.6°C ± 1.2°C) and MIS 22 (7.4°C ± 1.6°C, Figure 2b), crucial stages of ice-sheet build up during the MPT (Ford & Raymo, 2019), in particular of the European Ice Sheet (Berger & Jansen, 1994; Knudsen et al., 2020).

4.2. Heat Transfer Into the High Latitude North Atlantic During the MPT

Net northward heat transport to NENA was evaluated based on the horizontal SST gradient ($\Delta SST_{U1313\text{-}982}$; Figure 2c) between Site U1313 (Naafs et al., 2012) and subpolar Site 982 at 58°N (Lawrence et al., 2010). The evaluation of possible seasonality biases in alkenone-based SSTs suggests that these would not negatively impact our findings but rather reinforce them (cf. Texts S3 and S4).

Across the studied interval, $\Delta SST_{U1313\text{-}982}$ follows the same trend as our stratification index ($r = 0.69$, $p < 0.01$ using the Monte-Carlo-based surrogateCorr script implemented in the astrochron package in R; Meyers et al., 2014). Based on the modern annual SST difference between both sites (~7°C), we interpret the reduced $\Delta SST_{U1313\text{-}982}$ between MIS 24 and MIS 17 to reflect an increased net northward heat transport between subtropical and subpolar latitudes in the North Atlantic. The relatively mild and higher than average temperatures at Site 982 particularly during MIS 22 (Figure 3a) are notably at odds with the concurrent intrusion of subpolar waters in the mid-latitude North Atlantic as reflected by the high abundance of *Neogloboquadrina pachyderma* (Ruddiman et al., 1989, Figure 2d) and SST cooling at Site U1313 (Naafs et al., 2012). This indicates that the heat giving rise to mild SST at Site 982 between MIS 24 and MIS 17 was not transferred along a surface trajectory.

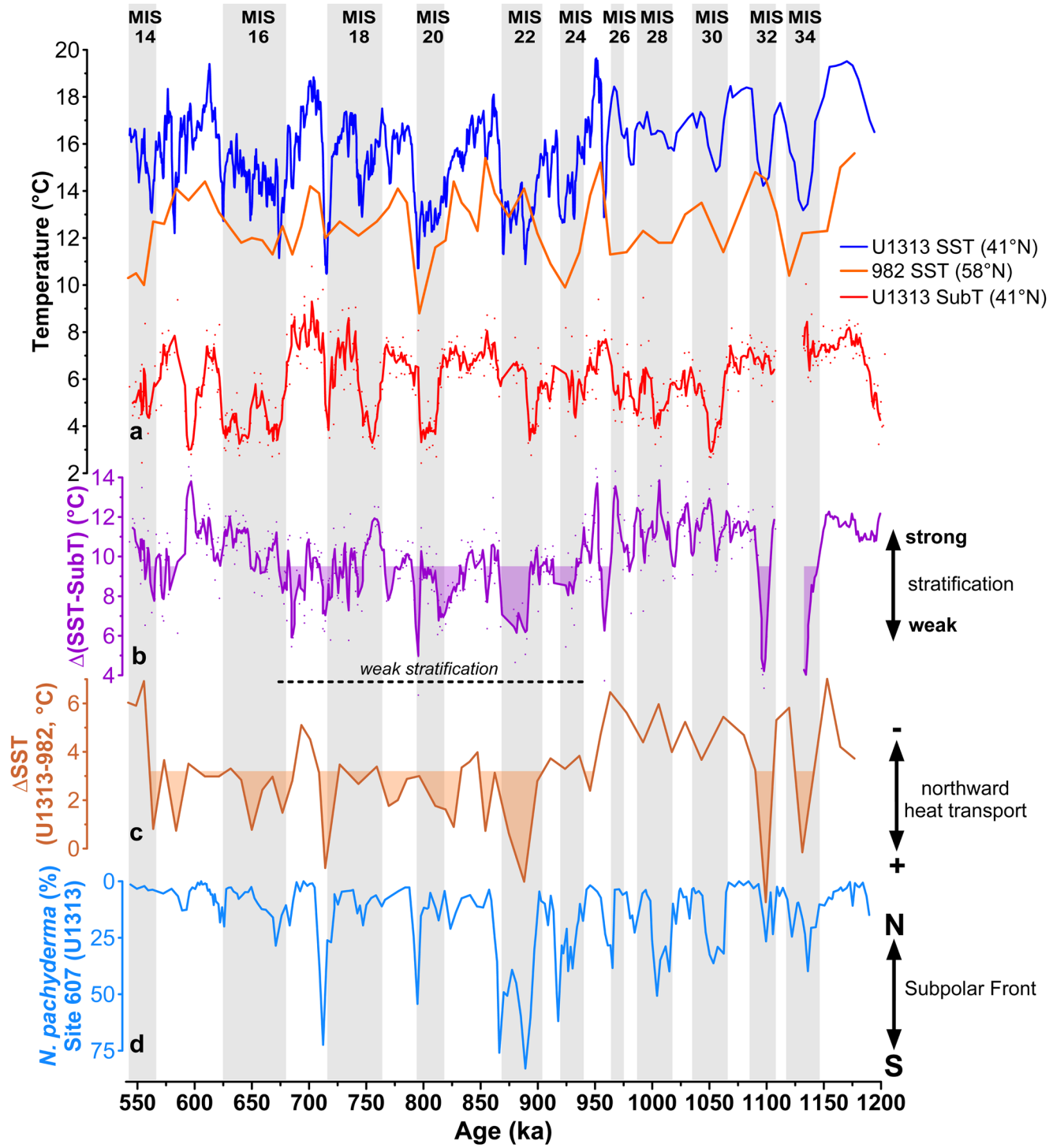

Figure 2. (a) Alkenone-based SSTs at Sites U1313 (blue, 3pt running mean; Naafs et al., 2012) and 982 (orange; Lawrence et al., 2010) and Mg/Ca-based SubT at Site U1313 (red, original data and 3 pt running mean; this study). (b) Upper-ocean stratification (Δ[SST-SubT]) at Site U1313 (original data and 3pt running mean). Purple shading marks stratification weaker (deeper thermocline) than the modern (9.5°C). Dashed line marks interval between 0.93 and 0.67 Ma (MISs 24–17). (c) Temperature gradient between Sites U1313 and 982. Shading marks $\Delta SST_{U1313\text{-}982}$ lower gradient than the study interval's average (3.2°C). (d) Percentage of *N. pachyderma* (Ruddiman et al., 1989) at Site 607.

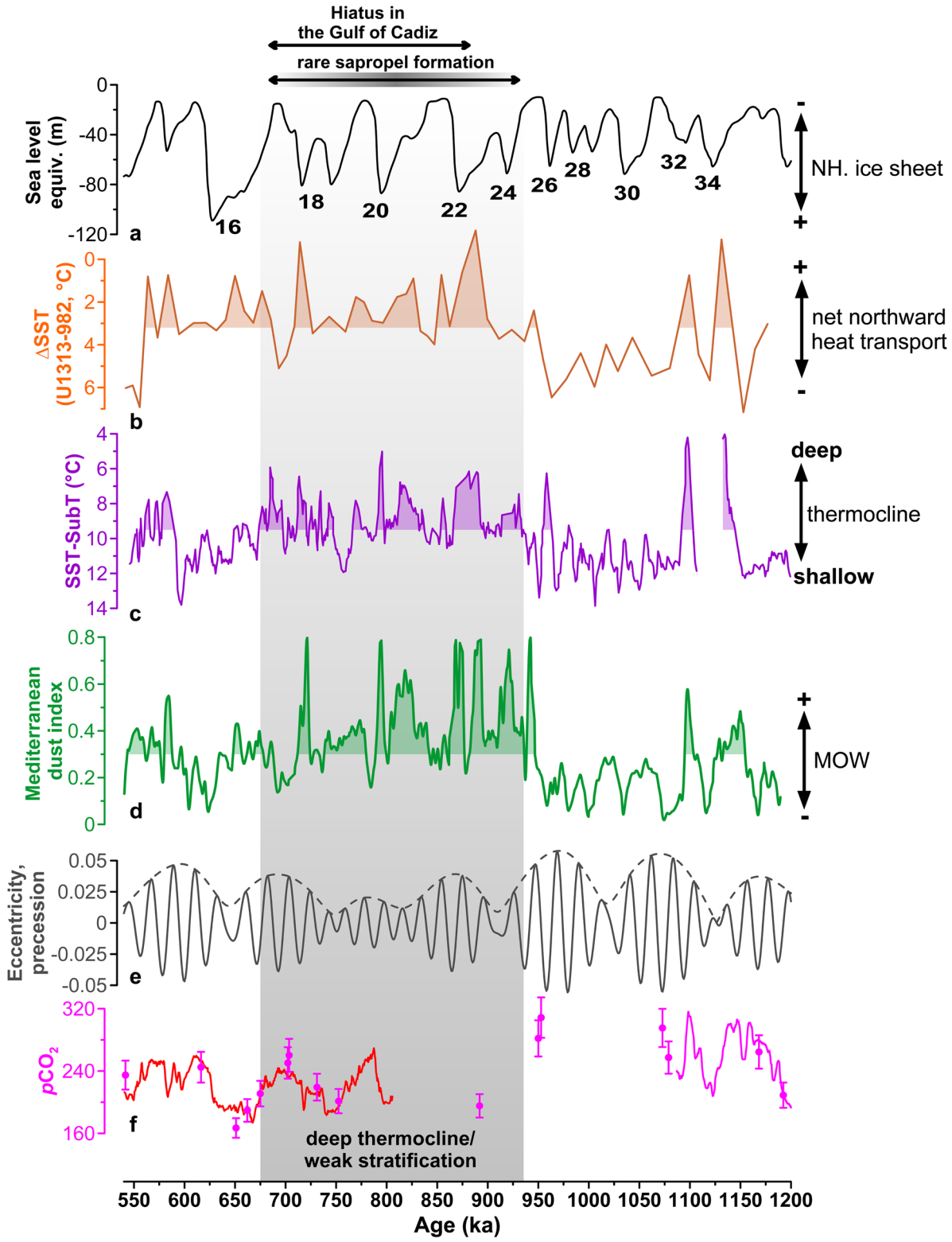

Figure 3. (a) Northern Hemisphere (NH) ice sheets sea-level equivalent (de Boer et al., 2014). (b) SST gradient between sites U1313 (Naafs et al., 2012) and 982 (Lawrence et al., 2010). (c) Thermocline stratification reflected by the Δ(SST-SubT) gradient at Site U1313. (d) Mediterranean dust index at Site 967 (Larrasoaña et al., 2003). (e) Eccentricity (dashed line) and precession parameters (solid line, Laskar et al., 2004). (f) Estimates of atmospheric pCO_2 (red line: Bereiter et al., 2015; pink symbols: Hönisch et al., 2009; pink line: Chalk et al., 2017).

4.3. Did Shifts in the Subpolar Front and/or Variations in AMOC Strength Cause the Subsurface Warming Between MIS 24 and MIS 17?

Temperature fluctuations in the upper ocean of the mid-latitude North Atlantic thermocline depth are typically attributed to spatial shifts of the Subpolar Front, as an expansion (retreat) of the front would decrease (increase) the influence of the STG above Site U1313, thereby cooling (warming) the entire upper water column. Such frontal shifts should therefore generate synchronous fluctuations of SST and SubT. However, particularly during MIS 24 and the end of MISs 22 and 20, SubT warmed while SST remained cold (Figures 2a and S5), arguing against frontal shifts as a driver of the SubT increases during these intervals.

The increased warming at depth with respect to the surface might instead be the consequence of a weakened Atlantic Meridional Overturning Circulation (AMOC; Lopes dos Santos et al., 2010); decreased inter-gyre heat transport would converge heat in the subtropics reducing thermal stratification in the upper ocean. As such, a weakened AMOC during the "900-kyr event" (Pena & Goldstein, 2014) could have contributed to thermocline deepening at our Site during MIS 24–22. However, we have two indications that the Δ(SST-SubT) variability was not primarily driven by fluctuations of AMOC strength: (a) The "900-kyr event" has been inferred to be a prolonged slowdown of ocean circulation centered around MIS 23, when the export of northern-sourced waters to the Southern Ocean was at its minimum (Pena & Goldstein, 2014). Temperature gradients at Site U1313, however, are comparable to modern (~9.5°C) during MIS 23, indicating that the thermocline was not particularly affected by a weak AMOC; (b) if Δ(SST-SubT) variability was driven by AMOC strength on orbital time scales, we would expect its spectral signal to peak in the obliquity band (Lisiecki, 2008; Rutberg & Broccoli, 2019). However, our Δ(SST-SubT) record is dominated by a peak in the precession frequency, without any obliquity imprint (Figure S6). This finding supports the assumption that AMOC strength is not the primary driver of the temperature gradient in the subtropical North Atlantic during the MPT.

4.4. Did Increased MOW Production Cause Thermocline Warming During the MPT?

We argue that the influence of the MOW on the deep-thermocline waters at Site U1313 is primarily responsible for the SubT warming during MIS 24–17 and induces the precession modulation of the Δ(SST-SubT) record. The MOW is a particularly suitable candidate to explain the good agreement between thermocline warming and increased northward heat transport to SPG because it affects temperature and salinity at deep-thermocline and upper-intermediate levels of both subtropical and subpolar North Atlantic (Potter & Lozier, 2004), thus playing a crucial role in determining upper-ocean stratification (Feucher et al., 2016).

Today, MOW mostly originates from warm and saline intermediate-depth waters formed in the Eastern Mediterranean that exit the Mediterranean Sea through the Strait of Gibraltar. Upon its passing through the Strait of Gibraltar, MOW warms the deep subtropical thermocline in eastern North Atlantic by intensely entraining the surrounding central waters (Baringer & Price, 1999), the residual Antarctic Intermediate Water (Reid, 1994), and by the release and decay of mesoscale eddies (Arhan & King, 1995; Bashmachnikov et al., 2015). Topographic control in the Gulf of Cadiz divides the MOW into a westward branch and northward branch, with the latter flowing at around 700 m water depth as an eastern boundary undercurrent along the European continental margin to the Irish Seas and Rockall Trough (Baringer & Price, 1999). There, it interacts with the North Atlantic Current due to upward sloping isopycnals and deep mixing in the eastern SPG (Pollard et al., 1996). Together, the warming effect of both branches effectively decreases thermocline stratification in eastern North Atlantic (Jia et al., 2007), increasing thermocline depth, and connecting western subtropics to NENA through density layers (Figure S2). This subsurface inter-gyre connection creates a pathway for isopycnal transport of thermohaline anomalies.

On orbital time scales, the production of MOW strongly depends on the aridity in the Eastern Mediterranean realm, which is driven by strength of the African Monsoon (AfM, Rohling et al., 2015) (cf. Text S5). During increased NH insolation (precession minima), the Intertropical Convergence Zone migrates northward and strengthens the AfM (Rohling et al., 2002). This strengthening leads to increased freshwater outflow by the River Nile decreasing surface salinity and buoyancy at the source region of the MOW (Bahr et al., 2015; Rohling et al., 2015). In turn, under a weaker AfM (precession maxima) and reduced continental fresh-water run-off, MOW production intensifies. This direct connection between MOW and AfM variability imprints a

strong and persistent precession-beat into MOW production (Bahr et al., 2015), which is also evident from the prevalence of precession (next to obliquity) in the cross-spectrum between Δ(SST-SubT) and the Mediterranean dust index (Figure S7).

Pronounced and widespread erosional features within the contourite system in the Gulf of Cadiz indicate strong outflow of the Mediterranean during the MPT (Hernandez-Molina et al., 2014; Lofi et al., 2016). This is further supported by increased dust influx toward the eastern Mediterranean Sea between MIS 25 and MIS 17 suggesting the prevalence of arid conditions in northeast Africa, which would have facilitated strong MOW production (Larrasoaña et al., 2003, Figures 3 and S8). This period also aligns with a scarcity of sapropels in the Eastern Mediterranean (Figure 3d and Konijnendijk et al., 2014), suggesting diminished runoff by the River Nile (Rohling et al., 2015). The presumed strengthening of MOW production during this interval also coincides with a period of flourishing cold-water coral reefs at the Irish Margin after a 600 kyr-long hiatus (Kano et al., 2007). These corals depend on the high-energy pycnocline between MOW and central waters for nutrient mobilization and larval dispersal, serving as indicators of MOW's northward branch presence along the eastern European margins (Wienberg et al., 2020).

The enhanced MOW production during MIS 25–17 is likely the result of the minimum of the ∼2.4 Myr eccentricity cycle at ∼930 ka. Low eccentricity led to reduced precession amplitudes, a weakened AfM, and thus favored conditions ideally suited to sustain a strong MOW production. This in turn would have kept the deep thermocline in the subtropical North Atlantic relatively warm even during times of decreasing atmospheric pCO_2 (Hönisch et al., 2009) and global surface-water cooling (McClymont et al., 2013). Increased subsurface heat advection to SPG, counteracting surface cooling, would lead to weaker thermocline stratification in central and northeastern North Atlantic, thus, creating a subsurface channel for latitudinal heat transport via the deep thermocline.

4.5. Further Implications: Impact of the Subsurface Heat Channel on Ice-Sheet Growth

Subsurface transport of warm waters to eastern SPG has the potential to impact adjacent ice-sheets. Within glacials stages with intermediate-sized ice sheets, warming of the eastern subpolar gyre could provide the moisture necessary to promote ice-sheet build up. To evaluate if the anomalously strong subsurface heat transport into the high latitudes during the MPT could provide additional moisture and thus enhance NH ice-sheet growth, we have conducted two glacial simulations with an atmospheric global-circulation model. The initial settings of both control (A_CTL) and experiment (A_WARM) simulations reflected intermediate glacial conditions with global ice-sheet volumes consistent with pre-MIS 22 glaciations (∼65 m sea level equivalent, Zhang et al., 2014; see supporting Text S6 and Figures 4 and S9). The experiment run was forced with a 2°C higher mean SST at NENA. This 2°C warming is the average SST difference at Site 982 between the glacial interval with lowest net northward heat transport (MIS 26; ∼11°C, Lawrence et al., 2010) and the glacial with maximum subsurface warming and maximum northward heat transport (MIS 22; ∼13°C). According to our model output, warming the subpolar North Atlantic by 2°C during intermediate glacial conditions boosts atmospheric absolute humidity, as well as stimulates a low-pressure anomaly across the NENA (Figure 4c). This in turn leads to enhanced moisture transport and a salient increase in annual mean precipitation over the Eurasian ice-sheets (Figure 4b) without evident changes in ice-sheet surface melting (Figure 4a). Based on this precipitation increase, our model output suggests that SST warming at NENA would have led to at least 3 m equivalent sea level of additional ice-volume growth. This is a conservative estimate because ice-sheet volumes were fixed in our simulations.

The increased northward subsurface heat transport against the cold atmospheric background associated with decreased glacial atmospheric CO_2 and intermediate-sized ice sheets ultimately provided a potent moisture source as evidenced by our model results and acted as an amplifier for NH ice-sheet growth over the strongly eroded regolith (Clark & Pollard, 1998; Clark et al., 2006). The resultant ice-sheet enlargement thus might have played a pivotal role for the cryosphere system to cross the critical threshold that enabled the full establishment of the large Late Pleistocene ice sheets after ∼700 ka BP.

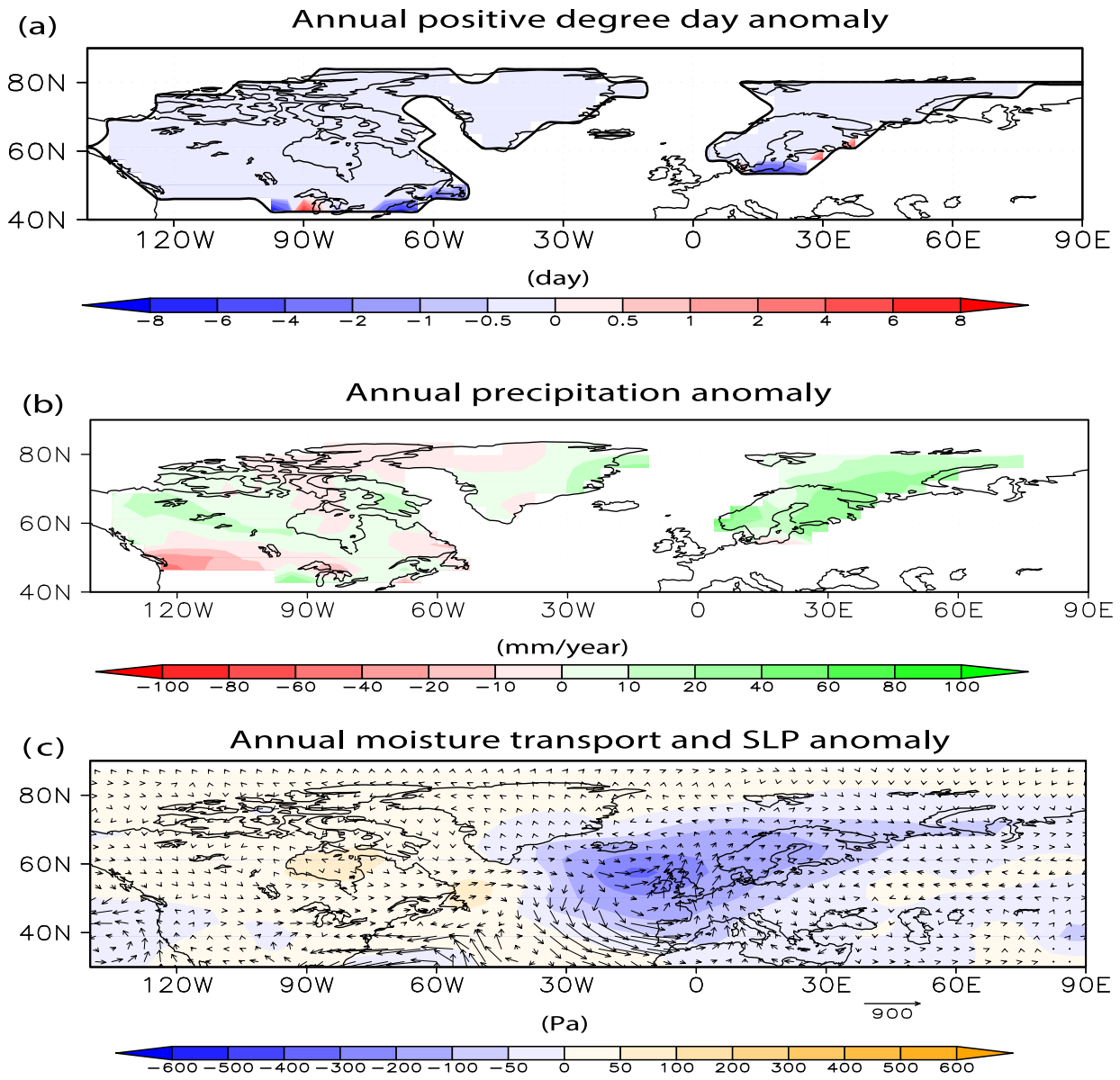

Figure 4. Changes in (a) Simulated changes in the annual mean positive degree days (units: day), (b) The annual mean precipitation (units: mm/year), (c) sea-level pressure (SLP, shaded, units: Pa), and vertical integrated moisture transport (vector, units: kg m^{-1} s^{-1}) in response to sea-surface warming in the northeastern North Atlantic in the climate model (Figure S9).

5. Conclusions

Here we describe a new precession-paced mechanism for the subsurface transport of warm waters to the eastern SPG during the MPT. Strong outflow of the Mediterranean Sea during the MPT deepened the thermocline in subtropical North Atlantic and led to the return of the MOW's northward branch to the eastern SPG, connecting the gyres along density layers. Increased inter-gyre connectivity allowed for the advection of warm waters to NENA at a time of presumably lower atmospheric temperatures, due to decreased glacial atmospheric CO_2 and southward shift of the SPG. Within glacial stages with intermediate-sized ice-sheets, a warming of the eastern SPG could have provided the moisture necessary to promote precipitation over ice-sheets downstream, particularly over the European Ice Sheets. As the advection of subtropical waters into the North Atlantic was essentially driven by orbital precession via the MOW, the combination of both the intrinsic obliquity forcing of ice-sheet feedbacks (Imbrie et al., 1993) and the precession-paced changes

in North Atlantic stratification might explain the averaged 100-kyr cyclicity that characterizes the post-MPT world (Feng & Bailer-Jones, 2015).

Conflict of Interest

The authors declare no conflicts of interest relevant to this study.

Data Availability Statement

All produced data is available in the supporting information, at ZENODO (https://doi.org/10.5281/zenodo.4738597) and has been submitted to the PANGAEA database.

Acknowledgments
The authors thank two anonymous reviewers for their careful reading of our manuscript, constructive comments, and suggestions. This research used samples and/or data provided by the International Ocean Discovery Program (IODP). We thank R. Kühn, M. Sutton, S. Schroeder, and J. Plale for laboratory assistance, and C. Scholz and S. Rheinberger for support during ICP-OES measurements. M. C. A. Catunda thanks F.W.C. and J.P.B. for mentoring; M. C. A. Catunda and A. Bahr were funded by DFG project BA 3809/8, O.F. by DFG project FR 2544/11. S. Kaboth-Bahr acknowledges an Open-Topic Post-Doc Grant from the University of Potsdam. X.Z. was funded via the Lanzhou University (project 225000–830006) and National Science Foundation of China (Grant 42075047). N.F. was funded by the NSF Grant 1756361. Open access funding enabled and organized by Projekt DEAL.

References

Arhan, M., & King, B. (1995). Lateral mixing of the Mediterranean water in the eastern North Atlantic. *Journal of Marine Research*, *53*, 865–895. https://doi.org/10.1357/0022240953212990

Bahr, A., Kaboth, S., Jiménez-Espejo, F. J., Sierro, F. J., Voelker, A. H. L., Lourens, L., et al. (2015). Persistent monsoonal forcing of Mediterranean outflow water dynamics during the late Pleistocene. *Geology*, *43*(11), 951–954. https://doi.org/10.1130/g37013.1

Baringer, M. O., & Price, J. F. (1999). A review of the physical oceanography of the Mediterranean outflow. *Marine Geology*, *155*(1–2), 63–82. https://doi.org/10.1016/s0025-3227(98)00141-8

Bashmachnikov, I., Neves, F., Calheiros, T., & Carton, X. (2015). Properties and pathways of Mediterranean water eddies in the Atlantic. *Progress in Oceanography*, *137*, 149–172. https://doi.org/10.1016/j.pocean.2015.06.001

Bereiter, B., Eggleston, S., Schmitt, J., Nehrbass-Ahles, C., Stocker, T. F., Fischer, H., et al. (2015). Revision of the EPICA Dome C CO2 record from 800 to 600 kyr before present. *Geophysical Research Letters*, *42*(2), 542–549. https://doi.org/10.1002/2014gl061957

Berger, W. H., & Jansen, E. (1994). Mid-Pleistocene climate shift-the Nansen connection. *In The Polar oceans and their role in shaping the global Environment* (Vol. 4, pp. 295–311).

Bower, A., Lozier, S., Biastoch, A., Drouin, K., Foukal, N., Furey, H., et al. (2019). Lagrangian views of the pathways of the Atlantic Meridional Overturning Circulation. *Journal of Geophysical Research: Oceans*, *124*(8), 5313–5335. https://doi.org/10.1029/2019jc015014

Brambilla, E., Talley, L. D., & Robbins, P. E. (2008). Subpolar Mode Water in the northeastern Atlantic: 2. Origin and transformation. *Journal of Geophysical Research*, *113*(C4), C04025. https://doi.org/10.1029/2006JC004063

Broecker, W. S. (1991). The great ocean conveyor. *Oceanography*, *4*(2), 79–89.

Burkholder, K. C., & Lozier, M. S. (2011). Subtropical to subpolar pathways in the North Atlantic: Deductions from Lagrangian trajectories. *Journal of Geophysical Research*, *116*(C7), C07017. https://doi.org/10.1029/2010jc006697

Burkholder, K. C., & Lozier, M. S. (2014). Tracing the pathways of the upper limb of the North Atlantic meridional overturning circulation. *Geophysical Research Letters*, *41*(12), 4254–4260. https://doi.org/10.1002/2014gl060226

Chalk, T. B., Hain, M. P., Foster, G. L., Rohling, E. J., Sexton, P. F., Badger, M. P., et al. (2017). Causes of ice age intensification across the Mid-Pleistocene transition. *Proceedings of the National Academy of Sciences*, *114*(50), 13114–13119. https://doi.org/10.1073/pnas.1702143114

Clark, P. U., Archer, D., Pollard, D., Blum, J. D., Rial, J. A., Brovkin, V., et al. (2006). The middle Pleistocene transition: Characteristics, mechanisms, and implications for long-term changes in atmospheric pCO_2. *Quaternary Science Reviews*, *25*(23–24), 3150–3184. https://doi.org/10.1016/j.quascirev.2006.07.008

Clark, P. U., & Pollard, D. (1998). Origin of the middle Pleistocene transition by ice sheet erosion of regolith. *Paleoceanography*, *13*(1), 1–9. https://doi.org/10.1029/97pa02660

Cléroux, C., deMenocal, P., Arbuszewski, J., & Linsley, B. (2013). Reconstructing the upper water column thermal structure in the Atlantic Ocean. *Paleoceanography*, *28*(3), 503–516. https://doi.org/10.1002/palo.20050

Daniault, N., Mazé, J. P., & Arhan, M. (1994). Circulation and mixing of Mediterranean Water west of the Iberian Peninsula. *Deep Sea Research I: Oceanographic Research Papers*, *41*(11–12), 1685–1714. https://doi.org/10.1016/0967-0637(94)90068-x

de Boer, B., Lourens, L. J., & van de Wal, R. S. W. (2014). Persistent 400,000-year variability of Antarctic ice volume and the carbon cycle is revealed throughout the Plio-Pleistocene. *Nature Communications*, *5*(2999). https://doi.org/10.1038/ncomms3999

Feng, F., & Bailer-Jones, C. A. L. (2015). Obliquity and precession as pacemakers of Pleistocene deglaciations. *Quaternary Science Reviews*, *122*, 166–179. https://doi.org/10.1016/j.quascirev.2015.05.006

Feucher, C., Maze, G., & Mercier, H. (2016). Mean structure of the North Atlantic subtropical permanent Pycnocline from in situ observations. *Journal of Atmospheric and Oceanic Technology*, *33*(6), 1285–1308. https://doi.org/10.1175/jtech-d-15-0192.1

Ford, H. L., & Raymo, M. E. (2019). Regional and global signals in seawater $\delta^{18}O$ records across the mid-Pleistocene transition. *Geology*, *48*(2), 113–117. https://doi.org/10.1130/g46546.1

Foukal, N. P., & Lozier, M. S. (2016). No inter-gyre pathway for sea-surface temperature anomalies in the North Atlantic. *Nature Communications*, *7*(11333), 1–6. https://doi.org/10.1038/ncomms11333

García-Ibáñez, M. I., Pérez, F. F., Lherminier, P., Zunino, P., Mercier, H., & Tréguer, P. (2018). Water mass distributions and transports for the 2014 GEOVIDE cruise in the North Atlantic. *Biogeosciences*, *15*(7), 2075–2090. https://doi.org/10.5194/bg-15-2075-2018

Greaves, M., Caillon, N., Rebaubier, H., Bartoli, G., Bohaty, S., Cacho, I., et al. (2008). Interlaboratory comparison study of calibration standards for foraminiferal Mg/Ca thermometry. *Geochemistry, Geophysics, Geosystems*, *9*(8), 1–27. https://doi.org/10.1029/2008GC001974

Hernandez-Molina, F. J., Stow, D. A. V., Avarez-Zarikian, C. A., Acton, G., Bahr, A., Balestra, B., et al. (2014). Onset of Mediterranean outflow into the North Atlantic. *Science*, *344*(6189), 1244–1250. https://doi.org/10.1126/science.1251306

Hodell, D., & Channell, J. (2016). Mode transitions in Northern Hemisphere glaciation: Co-evolution of millennial and orbital variability in Quaternary climate. *Climate of the Past*, *12*, 1805–1828. https://doi.org/10.5194/cp-12-1805-2016

Hönisch, B., Hemming, N. G., Archer, D., Siddall, M., & McManus, J. F. (2009). Atmospheric carbon dioxide concentration across the Mid-Pleistocene Transition. *Science*, *324*(5934), 1551–1554. https://doi.org/10.1126/science.1171477

Imbrie, J., Berger, A., Boyle, E. A., Clemens, S. C., Duffy, A., Howard, W. R., et al. (1993). On the structure and origin of major glaciation cycles 2. The 100,000-year cycle. *Paleoceanography*, *8*(6), 699–735. https://doi.org/10.1029/93pa02751
Jia, Y., Coward, A. C., de Cuevas, B. A., Webb, D. J., & Drijfhout, S. S. (2007). A model analysis of the behavior of the Mediterranean water in the North Atlantic. *Journal of Physical Oceanography*, *37*(3), 764–786. https://doi.org/10.1175/jpo3020.1
Kaboth-Bahr, S., Bahr, A., Zeeden, C., Toucanne, S., Eynaud, F., Jiménez-Espejo, F., et al. (2018). Monsoonal forcing of European ice-sheet dynamics during the late Quaternary. *Geophysical Research Letters*, *15*(11), 3145–7074.
Kano, A., Ferdelman, T. G., Williams, T., Henriet, J.-P., Ishikawa, T., Kawagoe, N., et al. (2007). Age constraints on the origin and growth history of a deep-water coral mound in the northeast Atlantic drilled during Integrated Ocean Drilling Program Expedition 307. *Geology*, *35*(11), 1051. https://doi.org/10.1130/g23917a.1
Kemle-von Mücke, S., & Oberhänsli, H. (1999). The distribution of living Planktic foraminifera in relation to Southeast Atlantic oceanography. *In Use of proxies in paleoceanography* (Vol. 53/2, pp. 91–115). Berlin, Heidelberg: Springer. https://doi.org/10.1007/978-3-642-58646-0_3
Knudsen, M. F., Nørgaard, J., Grischott, R., Kober, F., Egholm, D. L., Hansen, T. M., & Jansen, J. D. (2020). New cosmogenic nuclide burial-dating model indicates onset of major glaciations in the Alps during Middle Pleistocene Transition. *Earth and Planetary Science Letters*, *549*, 116491. https://doi.org/10.1016/j.epsl.2020.116491
Konijnendijk, T. Y. M., Ziegler, M., & Lourens, L. J. (2014). Chronological constraints on Pleistocene sapropel depositions from high-resolution geochemical records of ODP Sites 967 and 968. *Newsletters on Stratigraphy*, *47*(3), 263–282. https://doi.org/10.1127/0078-0421/2014/0047
Larrasoaña, J. C., Roberts, A. P., Rohling, E. J., Winklhofer, M., & Wehausen, R. (2003). Three million years of monsoon variability over the northern Sahara. *Climate Dynamics*, *21*(7–8), 689–698. https://doi.org/10.1007/s00382-003-0355-z
Laskar, J., Robutel, P., Joutel, F., Gastineau, M., Correia, A. C. M., & Levrard, B. (2004). A long-term numerical solution for the insolation quantities of the Earth. *Astronomy and Astrophysics*, *428*(1), 261–285. https://doi.org/10.1051/0004-6361:20041335
Lawrence, K. T., Sosdian, S., White, H. E., & Rosenthal, Y. (2010). North Atlantic climate evolution through the Plio-Pleistocene climate transitions. *Earth and Planetary Science Letters*, *300*(3–4), 329–342. https://doi.org/10.1016/j.epsl.2010.10.013
Lisiecki, L. E., Raymo, M. E., & Curry, W. B. (2008). Atlantic overturning responses to Late Pleistocene climate forcings. *Nature*, *456*(7218), 85–88. https://doi.org/10.1038/nature07425
Locarnini, M., Mishonov, A. V., Baranova, O. K., Boyer, T. P., Zweng, M. M., Garcia, H. E., et al. (2019). *World Ocean Atlas 2018, volume 1: Temperature*. NOAA Atlas NESDIS. https://doi.org/10.18142/228
Lofi, J., Voelker, A. H. L., Ducassou, E., Hernández-Molina, F. J., Sierro, F. J., Bahr, A., et al. (2016). Quaternary chronostratigraphic framework and sedimentary processes for the Gulf of Cadiz and Portuguese Contourite depositional systems derived from natural gamma ray records. *Marine Geology*, *377*, 40–57. https://doi.org/10.1016/j.margeo.2015.12.005
Lopes dos Santos, R. A., Prange, M., Castañeda, I. S., Schefuß, E., Mulitza, S., Schulz, M., et al. (2010). Glacial-interglacial variability in Atlantic meridional overturning circulation and thermocline adjustments in the tropical North Atlantic. *Earth and Planetary Science Letters*, *300*(3–4), 407–414. https://doi.org/10.1016/j.epsl.2010.10.030
Martin, P. A., & Lea, D. W. (2002). A simple evaluation of cleaning procedures on fossil benthic foraminiferal Mg/Ca. *Geochemistry, Geophysics, Geosystems*, *3*(10), 1–8. https://doi.org/10.1029/2001GC000280
McClymont, E. L., Sosdian, S. M., Rosell-Melé, A., & Rosenthal, Y. (2013). Pleistocene sea-surface temperature evolution: Early cooling, delayed glacial intensification, and implications for the mid-Pleistocene climate transition. *Earth-Science Reviews*, *123*, 173–193. https://doi.org/10.1016/j.earscirev.2013.04.006
Meyers, S. (2014). *Astrochron: An R package for astrochronology*. Retrieved from https://org/web/packages/astrochron/index.html
Naafs, B. D. A., Hefter, J., Acton, G., Haug, G. H., Martínez-Garcia, A., Pancost, R., & Stein, R. (2012). Strengthening of North American dust sources during the late Pliocene (2.7Ma). *Earth and Planetary Science Letters*, *317–318*, 8–19. https://doi.org/10.1016/j.epsl.2011.11.026
Pena, L. D., & Goldstein, S. L. (2014). Thermohaline circulation crisis and impacts during the mid-Pleistocene transition. *Science*, *345*(6194), 318–322. https://doi.org/10.1126/science.1249770
Pollard, R. T., Griffttths, M. J., Cunningham, S. A., Read, J. F., Pérez, F. F., & Ríos, A. F. (1996). Vivaldi 1991—A study of the formation, circulation and ventilation of eastern North Atlantic Central Water. *Progress in Oceanography*, *37*(2), 167–192. https://doi.org/10.1016/s0079-6611(96)00008-0
Potter, R. A., & Lozier, M. S. (2004). On the warming and salinification of the Mediterranean outflow waters in the North Atlantic. *Geophysical Research Letters*, *31*(1), L01202. https://doi.org/10.1029/2003GL018161
Raymo, M. E. (1997). The timing of major climate terminations. *Paleoceanography*, *12*(4), 577–585. https://doi.org/10.1029/97pa01169
Reid, J. L. (1994). On the total geostrophic circulation of the North Atlantic Ocean: Flow patterns, tracers, and transports. *Progress in Oceanography*, *33*(1), 1–92. https://doi.org/10.1016/0079-6611(94)90014-0
Rohling, E. J., Cane, T. R., Cooke, S., Sprovieri, M., Bouloubassi, I., Emeis, K. C., et al. (2002). African monsoon variability during the previous interglacial maximum. *Earth and Planetary Science Letters*, *202*(1), 61–75. https://doi.org/10.1016/s0012-821x(02)00775-6
Rohling, E. J., Marino, G., & Grant, K. M. (2015). Mediterranean climate and oceanography, and the periodic development of anoxic events (sapropels). *Earth-Science Reviews*, *143*, 62–97. https://doi.org/10.1016/j.earscirev.2015.01.008
Ruddiman, W. F., & McIntyre, A. (1981). Oceanic mechanisms for amplification of the 23,000-year ice-volume cycle. *Science*, *212*(4495), 617–627. https://doi.org/10.1126/science.212.4495.617
Ruddiman, W. F., Raymo, M. E., Martinson, D. G., Clement, B. M., & Backman, J. (1989). Pleistocene evolution: Northern Hemisphere ice sheets and North Atlantic Ocean. *Paleoceanography*, *4*(4), 353–412. https://doi.org/10.1029/pa004i004p00353
Rutberg, R. L., & Broccoli, A. J. (2019). Response of the high-latitude southern hemisphere to precessional forcing: Implications for Pleistocene Ocean circulation. *Paleoceanography and Paleoclimatology*, *34*(7), 1–15. https://doi.org/10.1029/2019pa003598
Shakun, J. D., Raymo, M. E., & Lea, D. W. (2016). An early Pleistocene Mg/Ca-δ^{18}O record from the Gulf of Mexico: Evaluating ice sheet size and pacing in the 41-kyr world. *Paleoceanography*, *31*, 1011–1027. https://doi.org/10.1002/2016PA002956
Spall, M. A. (1999). A simple model of the large-scale circulation of Mediterranean Water and Labrador Sea Water. *Deep Sea Research Part II: Topical Studies in Oceanography*, *46*(1–2), 181–204. https://doi.org/10.1016/S0967-0645(98)00105-2
Wienberg, C., Titschack, J., Frank, N., De Pol-Holz, R., Fietzke, J., Eisele, M., et al. (2020). Deglacial upslope shift of NE Atlantic intermediate waters controlled slope erosion and cold-water coral mound formation (Porcupine Seabight, Irish margin). *Quaternary Science Reviews*, *237*, 106310. https://doi.org/10.1016/j.quascirev.2020.106310
Zhang, X., Lohmann, G., Knorr, G., & Purcell, C. (2014). Abrupt glacial climate shifts controlled by ice sheet changes. *Nature*, *512*(7514), 290–294. https://doi.org/10.1038/nature13592
Zweng, M., Seidov, D., Boyer, T., Locarnini, M., Garcia, H., Mishonov, A., et al. (2019). *World ocean atlas 2018, volume 2: Salinity*. NOAA Atlas NESDIS. https://doi.org/10.18142/228

References From the Supporting Information

Bahr, A., Nürnberg, D., Schönfeld, J., & Garbe-Schönberg, D. (2011). Hydrological variability in Florida straits during marine isotope Ssage 5 cold events. *Paleoceanography*, *26*, PA2214. https://doi.org/10.1029/2010PA002015

Bolton, C. T., Bailey, I., Friedrich, O., Tachikawa, K., Garidel-Thoron, T., Vidal, L., et al. (2018). North Atlantic midlatitude surface-circulation changes through the Plio-Pleistocene intensification of northern hemisphere glaciation. *Paleoceanography and Paleoclimatology*, *33*, 1186–1205. https://doi.org/10.1029/2018pa003412

Ferretti, P., Crowhurst, S. J., Naafs, B. D. A., & Barbante, C. (2015). The marine isotope stage 19 in the mid-latitude North Atlantic Ocean: Astronomical signature and intra-interglacial variability. *Quaternary Science Reviews*, *108*, 95–110. https://doi.org/10.1016/j.quascirev.2014.10.024

Hammer, Ø., Harper, D. A., & Ryan, P. D. (2001). PAST: Paleontological statistics software package for education and data analysis. *Palaeontologia Electronica*, *4*(1), 9.

Harvey, J. (1982). θ-S relationships and water masses in the eastern North Atlantic. *Deep Sea Research A: Oceanography Research. Papers*, *29*(8), 1021–1033. https://doi.org/10.1016/0198-0149(82)90025-5

Kaboth, S., de Boer, B., Bahr, A., Zeeden, C., & Lourens, L. J. (2017). Mediterranean outflow water dynamics during the past ∼570 kyr: Regional and global implications. *Paleoceanography*, *32*(6), 634–647. https://doi.org/10.1002/2016pa003063

Karas, C., Nürnberg, D., Bahr, A., Groeneveld, J., Herrle, J. O., Tiedemann, R., & Demenocal, P. B. (2017). Pliocene oceanic seaways and global climate. *Scientific Reports*, *7*(1), 1–8. https://doi.org/10.1038/srep39842

Konijnendijk, T. Y. M., Ziegler, M., & Lourens, L. J. (2015). On the timing and forcing mechanisms of late Pleistocene glacial terminations: Insights from a new high-resolution benthic stable oxygen isotope record of the eastern Mediterranean. *Quaternary Science Reviews*, *129*, 308–320. https://doi.org/10.1016/j.quascirev.2015.10.005

Lisiecki, L. E., & Raymo, M. E. (2005). A Pliocene-Pleistocene stack of 57 globally distributed benthic $\delta^{18}O$ records. *Paleoceanography*, *20*, PA1003. https://doi.org/10.1029/2004PA001071

Lozier, M. S., & Stewart, N. M. (2008). On the temporally varying northward penetration of Mediterranean overflow water and eastward penetration of Labrador Sea water. *Journal of Physical Oceanography*, *38*(9), 2097–2103. https://doi.org/10.1175/2008jpo3908.1

Mollenhauer, G., Kienast, M., Lamy, F., Meggers, H., Schneider, R. R., Hayes, J. M., & Eglinton, T. I. (2005). An evaluation of ^{14}C age relationships between co-occurring foraminifera, alkenones, and total organic carbon in continental margin sediments. *Paleoceanography*, *20*(1), PA1016. https://doi.org/10.1029/2004pa001103

Naafs, B. D. A., Hefter, J., Ferretti, P., Stein, R., & Haug, G. H. (2011). Sea surface temperatures did not control the first occurrence of Hudson Strait Heinrich Events during MIS 16. *Paleoceanography*, *26*(4), PA4201. https://doi.org/10.1029/2011PA002135

Naafs, B. D. A., Hefter, J., Gruetzner, J., & Stein, R. (2013). Warming of surface waters in the mid-latitude North Atlantic during Heinrich events. *Paleoceanography*, *28*(1), 153–163. https://doi.org/10.1029/2012pa002354

Paillard, D., Labeyrie, L., & Yiou, P. (2011). Macintosh program performs time-series analysis. *Eos Transactions American Geophysical Union*, *77*(39), 379. https://doi.org/10.1029/96eo00259

Paul, D., Skrzypek, G., & Fórizs, I. (2007). Normalization of measured stable isotopic compositions to isotope reference scales—a review. *Rapid Communications in Mass Spectrometry*, *21*(18), 3006–3014. https://doi.org/10.1002/rcm.3185

Reid, J. L. (1979). On the contribution of the Mediterranean Sea outflow to the Norwegian-Greenland Sea. *Deep Sea Research A: Oceanography Research Papers*, *26*(11), 1199–1223. https://doi.org/10.1016/0198-0149(79)90064-5

Robinson, R. S., Jones, C. A., Kelly, R. P., Rafter, P., Etourneau, J., & Martinez, P. (2019). A cool, nutrient-enriched eastern equatorial Pacific during the Mid-Pleistocene transition. *Geophysical Research Letters*, *46*(4), 2187–2195. https://doi.org/10.1029/2018gl081315

Roeckner, E., Bäuml, G., Bonaventura, L., Brokopf, R., Esch, M., Giorgetta, M., et al. (2003). *The atmospheric general circulation model ECHAM 5. PART I: Model description*. Report/Max-Plank-Institut für Meteorologie (p. 349).

Rosell-Melé, A., Eglinton, G., Pflaumann, U., & Sarnthein, M. (1995). Atlantic core top calibration of the $U_{37}^{K'}$ index as a sea-surface paleotemperature indicator. *Geochimica Cosmochimica Acta*, *59*, 3099–3107. https://doi.org/10.1016/0016-7037(95)00199-a

Samtleben, C., & Bickert, T. (1990). Coccoliths in sediment traps from the Norwegian Sea. *Marine Micropaleontology*, *16*, 39–64. https://doi.org/10.1016/0377-8398(90)90028-k

Schlitzer, R. (2002). Interactive analysis and visualization of geoscience data with ocean data view. *Computers & Geosciences*, *28*(10), 1211–1218. https://doi.org/10.1016/s0098-3004(02)00040-7

Schulz, M., & Mudelsee, M. (2002). REDFIT: Estimating red-noise spectra directly from unevenly spaced paleoclimatic time series. *Computers & Geosciences*, *28*(3), 421–426. https://doi.org/10.1016/s0098-3004(01)00044-9

Seo, I., Lee, Y. I., Kim, W., Yoo, C. M., & Hyeong, K. (2015). Movement of the Intertropical Convergence Zone during the mid-pleistocene transition and the response of atmospheric and surface ocean circulations in the central equatorial Pacific. *Geochemistry, Geophysics, Geosystems*, *16*(11), 3973–3981. https://doi.org/10.1002/2015gc006077

Sepulcre, S., Vidal, L., Tachikawa, K., Rostek, F., & Bard, E. (2011). Sea-surface salinity variations in the northern Caribbean Sea across the Mid-Pleistocene Transition. *Climate of the Past*, *7*(1), 75–90. https://doi.org/10.5194/cp-7-75-2011

Shackleton, N. J., & Opdyke, N. D. (1973). Oxygen isotope and paleomagnetic stratigraphy of Equatorial Pacific core V28-238: Oxygen isotope temperatures and ice volumes on a 10^5 year and 10^6 year scale. *Quaternary Research*, *3*(1), 39–55. https://doi.org/10.1016/0033-5894(73)90052-5

Trauth, M. H., Larrasoana, J. C.,& Mudelsee, M. (2009). Trends, rhythms and events in Plio-Pleistocene African climate. *Quaternary Science Reviews*, *28*(5–6), 399–411. https://doi.org/10.1016/j.quascirev.2008.11.003

Trauth, M. H., Maslin, M. A., Deino, A., & Strecker, M. R. (2005). Late Cenozoic moisture history of East Africa. *Science*, *309*(5743), 2051–2053. https://doi.org/10.1126/science.1112964